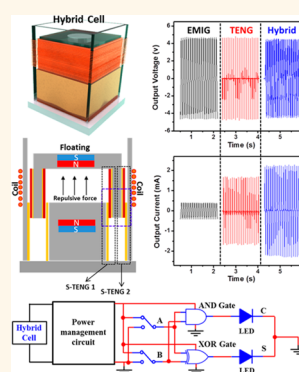# Hybridizing Triboelectrification and Electromagnetic Induction Effects for High-Efficient Mechanical Energy Harvesting

Youfan Hu,[†,‡,⊥] Jin Yang,[†,§,⊥] Simiao Niu,[†] Wenzhuo Wu,[†] and Zhong Lin Wang[†,∥],*

[†]School of Material Science and Engineering, Georgia Institute of Technology, Atlanta, Georgia 30332-0245, United States, [‡]Key Laboratory for the Physics and Chemistry of Nanodevices, and Department of Electronics, Peking University, Beijing 100871, China, [§]Department of Optoelectronic Engineering, Chongqing University, Chongqing 400044, China, and [∥]Beijing Institute of Nanoenergy and Nanosystems, Chinese Academy of Sciences, Beijing 100083, China. [⊥]Y. Hu and J. Yang contributed equally to this work.

ABSTRACT The recently introduced triboelectric nanogenerator (TENG) and the traditional electromagnetic induction generator (EMIG) are coherently integrated in one structure for energy harvesting and vibration sensing/isolation. The suspended structure is based on two oppositely oriented magnets that are enclosed by hollow cubes surrounded with coils, which oscillates in response to external disturbance and harvests mechanical energy simultaneously from triboelectrification and electromagnetic induction. It extends the previous definition of hybrid cell to harvest the same type of energy with multiple approaches. Both the sliding-mode TENG and contact-mode TENG can be achieved in the same structure. In order to make the TENG and EMIG work together, transformers are used to match the output impedance between these two power sources with very different characteristics. The maximum output power of 7.7 and 1.9 mW on the same load of 5 kΩ was obtained for the TENG and EMIG, respectively, after impedance matching. Benefiting from the rational design, the output signal from the TENG and the EMIG are in phase. They can be added up directly to get an output voltage of 4.6 V and an output current of 2.2 mA in parallel connection. A power management circuit was connected to the hybrid cell, and a regulated voltage of 3.3 V with constant current was achieved. For the first time, a logic operation was carried out on a half-adder circuit by using the hybrid cell working as both the power source and the input digit signals. We also demonstrated that the hybrid cell can serve as a vibration isolator. Further applications as vibration dampers, triggers, and sensors are all promising.

Mechanical energy is a huge resource in the ambient environment with various energy scales and types, such as the tide in the ocean, wind, falling water, machine vibration, flying aircrafts, walking, and many more. Generally, there are several approaches that can be used to convert mechanical energy into electrical energy, including by means of electromagnetic induction effect,[1,2] electrostatic effect,[3,4] and piezoelectric effect.[5−9] The electromagnetic induction phenomenon was first discovered in 1831, and the electromagnetic induction generator (EMIG) works as a dominant way to generate commercially significant quantities of electric power due to its high conversion efficiency and superior durability. Most recently, we

developed an innovative approach, a triboelectric nanogenerator (TENG), for harvesting ambient mechanical energy based on the coupling of the triboelectric effect and electrostatic induction.[10−14] When two materials with opposite triboelectric polarities are in periodic contact and separation, the induced electrons were alternately driven to flow between the top and bottom electrodes through external circuits. It has been proved to be a cost-effective, simple, and robust technology for energy harvesting and has been demonstrated to provide enough energy for self-powered mobile systems.

The TENG and EMIG have very different characteristics. The former has a large output impedance and can produce very high
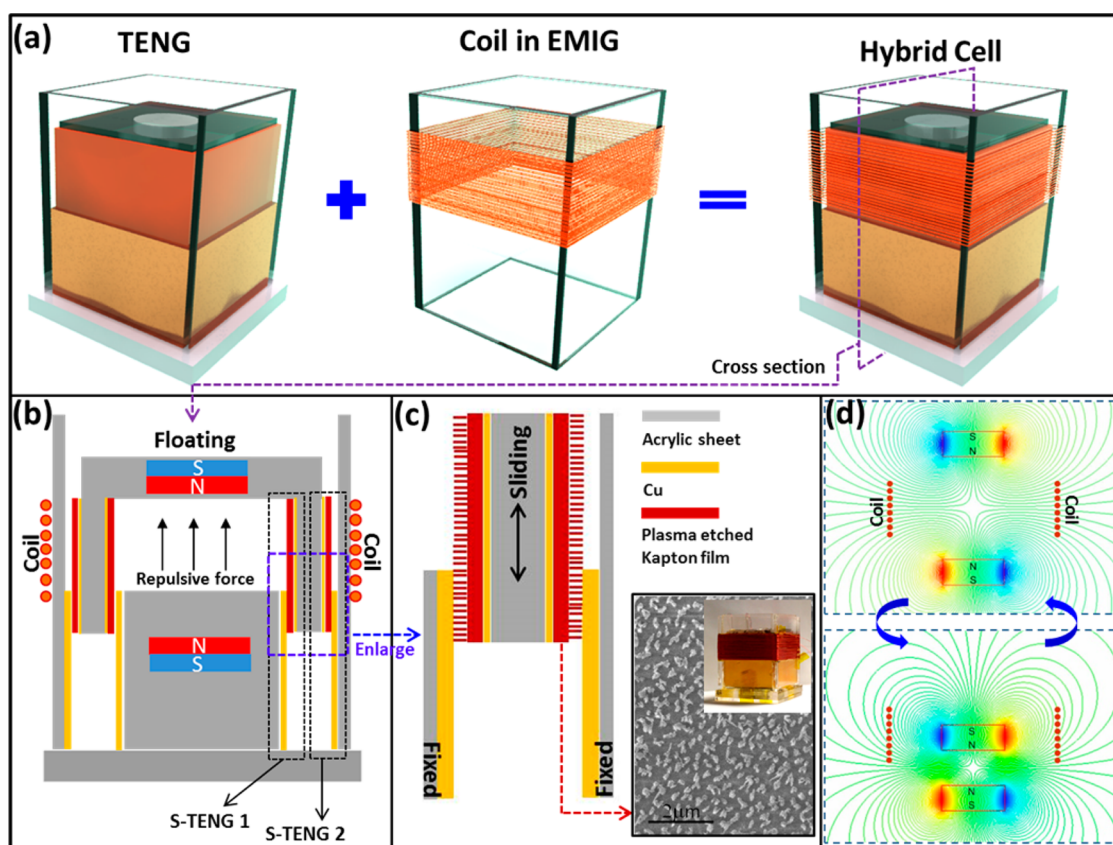
Figure 1. (a) Schematic diagram of the hybrid cell integrated with a sliding-mode TENG and EMIG. (b) Cross section view of the hybrid cell. The two dashed black boxes indicate the locations of two S-TENGs. (c) Enlarged view of the S-TENG structure circled by the purple dashed box in (b). The inset is the SEM image taken on the Kapton film's surface with nanowire structures and a photo of the real device. (d) Simulated magnetic field distribution. The distribution of magnetic field changes when the floating hollow cube oscillates.

voltage but low current, while the latter has a small output impedance, with high current but low voltage. The concept of a hybrid cell was proposed several years ago for harvesting multitype energies simultaneously from the environment using an integrated device structure.[15−19] This concept can be expanded for harvesting the same kind of energy by simultaneously using multiple types of generators based on different working mechanisms.[20,21] It is similar to using multiple solar cells that capture different wavelengths of light for full usage of the entire solar spectrum. One critical issue arising for a hybrid cell's practical application is the impedance match between different contributing parts when a load is added, which has not been discussed before. It will greatly limit the output capability of the hybrid cell as a power source.

In this work, with a rational design, the TENG and EMIG are integrated in a suspended structure as a hybrid cell. A moving part is floated by a repulsive force between two oppositely oriented magnets and can oscillate around a balance point in response to mechanical disturbance in the environment, which harvests mechanical energy simultaneously from triboelectrification and electromagnetic induction. Transformers are used to make the impedance match

between these two power sources and also to adjust the output voltages to a similar level. The maximum instantaneous output power of 7.7 and 1.9 mW on the same load of 5 kΩ was obtained for the TENG and EMIG, respectively. A power management circuit was used to convert the hybrid cell's ac output to a dc one. A regulated 3.3 V output voltage can be obtained and used to work as the power source and the input digit signals for the logic operation on a half-adder circuit. The application of the hybrid cell as a vibration isolator was demonstrated and shown to be good quality. Many other applications including vibration detection, vibration damping, vibration triggers, *etc.*, are all promising based on the design.

RESULTS AND DISCUSSION

A schematic diagram of a hybrid cell integrated with the TENG and EMIG is shown in Figure 1a. To clarify the device structure, Figure 1b shows the corresponding cross section view. The detailed fabrication process is described in the Methods section. The basic frame structure is a smaller hollow cube with an opening bottom floating in a larger hollow cube with an opening top. A solid cube is fixed on the bottom of the larger hollow cube. The side wall surfaces of the solid cube
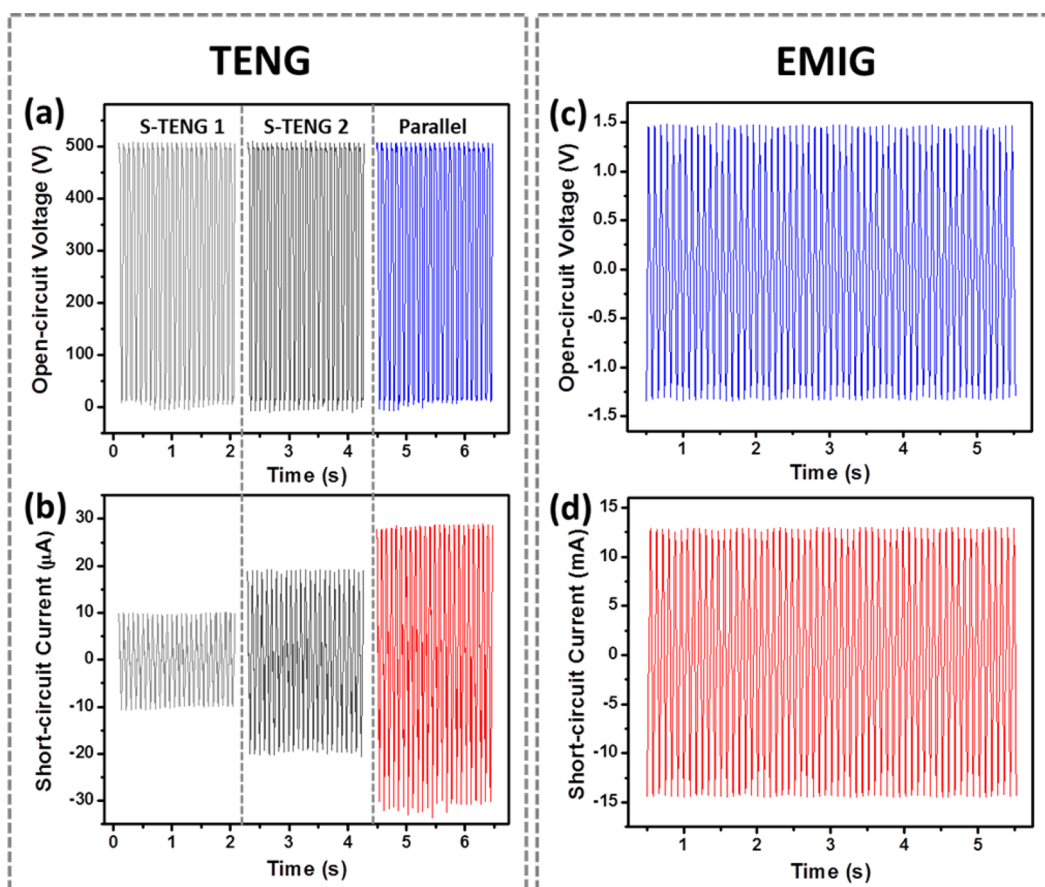
Figure 2. Output performance of the TENG and EMIG when they work simultaneously. (a) Open-circuit voltage and (b) short-circuit current of TENG. (c) Open-circuit voltage and (d) short-circuit current of EMIG.

and the lower part of the inner surfaces of the larger hollow cube are covered with copper foil. Both the inner and outer side wall surfaces of the smaller hollow cube are covered with Kapton film. The floating of the smaller hollow cube is maintained by the balance between its gravity and the repulsive force between two magnets embedded in the solid cube and the smaller hollow cube, respectively. The smaller hollow cube's side walls insert into the space between the solid cube and the larger hollow cube. The two contact surfaces construct two sliding-mode TENGs (S-TENGs), as indicated by two black dashed boxes in Figure 1b. The center working part is enlarged in Figure 1c. The copper foils work as a friction surface and also as an electrode in the S-TENG. The Kapton film's surface is treated with inductively coupled plasma (ICP) to create aligned nanowire structures, which can enhance the contact area with the copper foils. The average diameter of these nanowires is 100 ± 3 nm with an average length of 1.1 ± 0.4 μm. A thin copper film is deposited on the back surface of the Kapton film to work as the other electrode of the S-TENG. When there is a mechanical disturbance, the smaller hollow cube will oscillate up and down around a balance point. Thus, a relative sliding motion will be introduced between the copper foil and the Kapton film, and the

S-TENG starts to work. A varnished wire is wrapped on the outer surface of the larger hollow cube to construct a coil with 300 turns. When the floating hollow cube oscillates, the spatial distribution of the magnetic field introduced by the embedded magnets will be changed, as illustrated in Figure 1d based on numerical simulation. Thus, the magnetic flux in the coil will be altered, and an electromagnetic induction current is generated. This is the working mechanism of the EMIG.

Figure 2 shows the output performance of the TENG and EMIG when they work simultaneously. According to our previous theoretical modeling, the open-circuit voltage and short-circuit current of S-TENG in this case can be represented as[22]

$$V_{oc}^s = \frac{\sigma x d}{\varepsilon_0 \varepsilon_r (l - x)} \qquad (1)$$

$$I_{sc}^s = \sigma w \frac{dx}{dt} \qquad (2)$$

where σ is the surface density of triboelectric charges, x is the separation distance between the two friction surfaces, d is the thickness of the Kapton film, l is the geometric size in the vertical direction of the friction surfaces, w is the perimeter of the friction surface, ε_0 is the permittivity of the vacuum, and ε_r is the relative
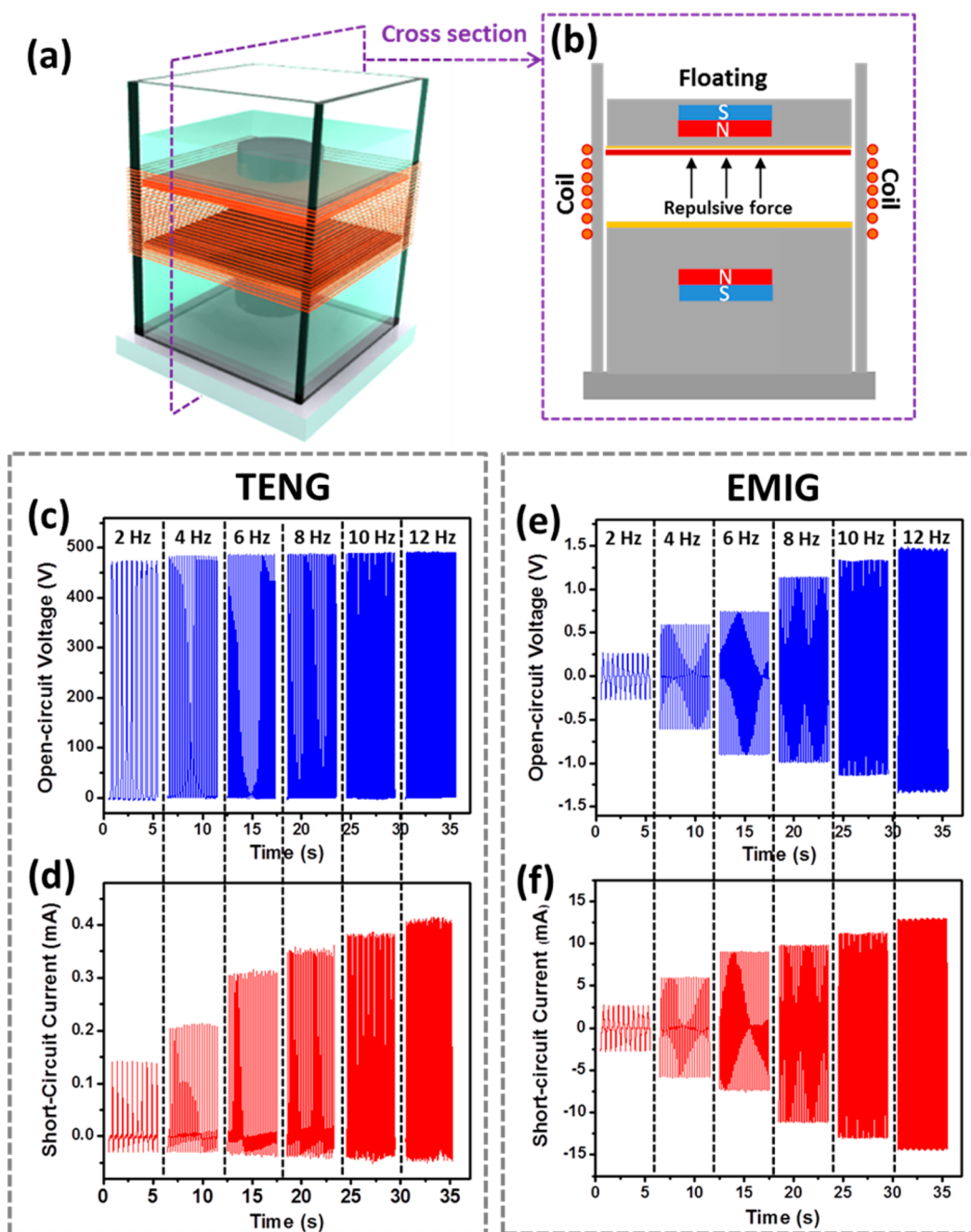
Figure 3. (a) Schematic diagram of the hybrid cell integrated with contacting-mode TENG and EMIG. (b) Cross section view of the hybrid cell. Frequency responses of (c) open-circuit voltage and (d) short-circuit current from TENG. Frequency response of (e) open-circuit voltage and (f) short-circuit current from EMIG.

permittivity of the Kapton film. Referring to the device structure and the working principle as shown in Figure 1c, the separation distance x, the geometric size l, and the thickness of the Kapton film in S-TENG 1 and S-TENG 2 are equal. As the friction surfaces in these two S-TENGs are identical, it is reasonable to assume that σ is the same for them. Thus, the open-circuit voltage should be the same in S-TENG 1 and S-TENG 2, which is the case as shown in Figure 2a. An open-circuit voltage of 500 V is achieved for both S-TENG 1 and S-TENG 2. For the short-circuit current, as the friction surfaces'

perimeter in S-TENG 2 is almost double that of the S-TENG 1, 18.9 and 10 μA was obtained for S-TENG 2 and S-TENG 1, respectively, as shown in Figure 2b. Because these two S-TENGs work synchronously, the output signals are in phase. When they are connected in parallel, the short-circuit currents were added, and the open-circuit voltage was maintained at 500 V.

For the EMIG, when the TENGs are working, there is relative motion between the magnet in the floating part and the coil, leading to the change of the magnetic field distribution in the coil. The electromagnetic
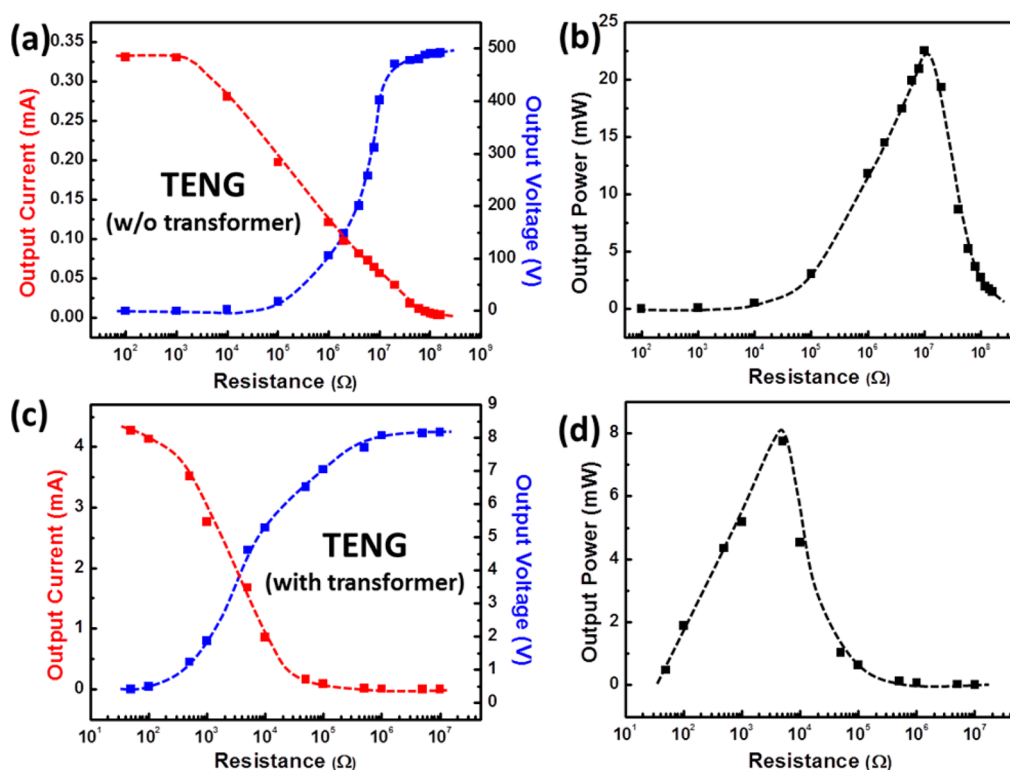
Figure 4. Original dependence of (a) the output voltage, current, and (b) instantaneous power on the load resistance of the TENG. After serially connecting with transformers, the dependence of (c) the output voltage, current, and (d) instantaneous power on the load resistance of the TENG. The output impedance of the TENG decreased from 10 MΩ to 5 kΩ.

induction induced open-circuit voltage is given by Faraday's law:

$$V_{oc}^{EM} = \int_0^m Bvdm \quad (3)$$

The short-circuit current is

$$I_{sc}^{EM} = \frac{V_{oc}^{EM}}{r} \quad (4)$$

in which B is the magnetic field, m is the coil length, and v is the velocity of the relative motion between the magnet and coil. r is the inner resistance of the coil. Working simultaneously with TENGs, the measured electromagnetic induction induced open-circuit voltage is around 1.5 V, and the short-circuit current in the coil is around 12.5 mA, as shown in Figure 2c and d, respectively.

In addition to the sliding-mode TENG, a contact-mode TENG (C-TENG) can also be integrated in this structure. Figure 3a and b show the device design and the corresponding cross section view, respectively. A solid cube embedded with a magnet is fixed on the bottom of a hollow cube with an opening on the top. The solid cube's top surface is covered with copper foil. Another solid cube embedded with magnets is floating above the fixed one with the bottom surface covered with Kapton film. A varnished wire is wrapped around the outer surface of the hollow cube to construct a coil with 300 turns. Since the mechanical energy has a wide

frequency distribution in the environment, especially in the low-frequency range, the dependence of the output performance on the working frequency is of interest. We tested the device with six different frequencies, from 2 to 12 Hz, with constant oscillation amplitude of the floating solid cube. Figure 3c–f show the results. For a contact-mode TENG, the open-circuit voltage and short-circuit current are given by[23]

$$V_{OC}^c = \frac{\sigma x}{\varepsilon_0} \quad (5)$$

$$I_{SC}^c = \frac{S\sigma d_0}{(d_0+x)^2} \frac{dx}{dt} \quad (6)$$

in which $d_0 = d/\varepsilon_r$. In this case, x is the distance between two contact surfaces. Because the oscillation amplitude of the floating part is fixed, the open-circuit voltage is almost the same for different frequencies, as shown in Figure 3c, while for the short-circuit current, it presents a very clear increasing trend with the increase of frequency, as shown in Figure 3d, which is due to the increased oscillation velocity. At a frequency of 12 Hz, the open-circuit voltage and short-circuit current for the TENG are around 490 V and 0.4 mA, respectively.

For the EMIG, according to eqs 3 and 4, the open-circuit voltage is proportional to the velocity of the relative motion between the magnet and coil. As the oscillation frequency increases, the relative motion
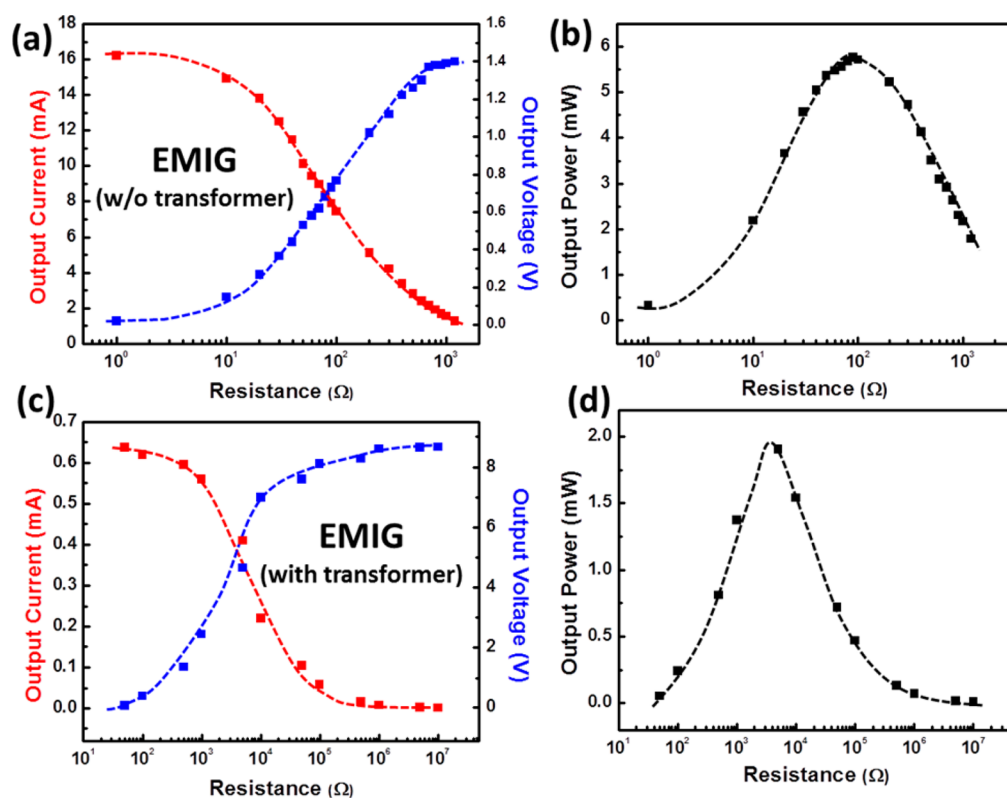
Figure 5. Original dependence of (a) the output voltage, current, and (b) instantaneous power on the load resistance of the EMIG. After serially connecting with transformers, the dependence of (c) the output voltage, current, and (d) instantaneous power on the load resistance of the EMIG. The output impedance of the EMIG increased from 90 Ω to 5 kΩ, matched with the TENG.

velocity increases. So the open-circuit voltage increases, and the short-circuit current also increases, which has a linear relationship with the open-circuit voltage, as shown in Figure 3e and f. At a frequency of 12 Hz, the open-circuit voltage and short-circuit current for the EMIG reached 1.5 V and 13 mA, respectively.

For an energy conversion device, when it is used to directly drive an electric device, working at the matched impedance can maximize the transferred power. We checked the output impedance of TENG and EMIG by recording the output performances of the TENG and EMIG when they are connected to a load with different resistances, as shown in Figure 4a and Figure 5a, respectively. The output current to the load decreases as the resistance increases, while the output voltage across the load increases as the resistance increases. The obtained maximum instantaneous output power is 22.5 mW at a load of 10 MΩ for the TENG (Figure 4b) and 5.8 mW with a load of 90 Ω for the EMIG (Figure 5b). When considering the power delivery capability, another issue raised for the hybrid cell is the impedance match between different contributing parts. Here we can see that the TENG and EMIG have very different characteristics. There are 4 orders of magnitude difference in output impedance between the TENG and EMIG. In such conditions, huge internal power consumption will exist in the hybrid cell itself

when these two parts are working together simultaneously, which is contrary to our original purpose of using a hybrid structure to enhance energy conversion efficiency. To solve this problem, transformers were used to get an impedance match between the TENG and EMIG. Figures 4c and 5c are the output voltage and current of the TENG and EMIG with transformers on various load resistance. The output impedance was adjusted to 5 kΩ for both the TENG and EMIG with the maximum instantaneous output power of 7.7 and 1.9 mW, as shown in Figures 4d and 5d, respectively. The transformers we used are commercial standard ones with a working frequency of 60 Hz. The energy transform efficiency declined quickly when it works at a frequency deviating from 60 Hz. In the test, the TENG and EMIG worked at a frequency of 12 Hz. The loss of power here mainly comes from the mismatch of the working frequency between them. This can be greatly improved if a proper transformer is chosen in future work.

A major advantage of this new hybrid cell is that due to the rational design, the output signals from both the TENG and EMIG are in phase. Thus, they can be added constructively and directly. Another important characteristic of the device after impedance match is that the output voltages from both the TENG and EMIG are adjusted to a similar level, around 4.6 V with a matched
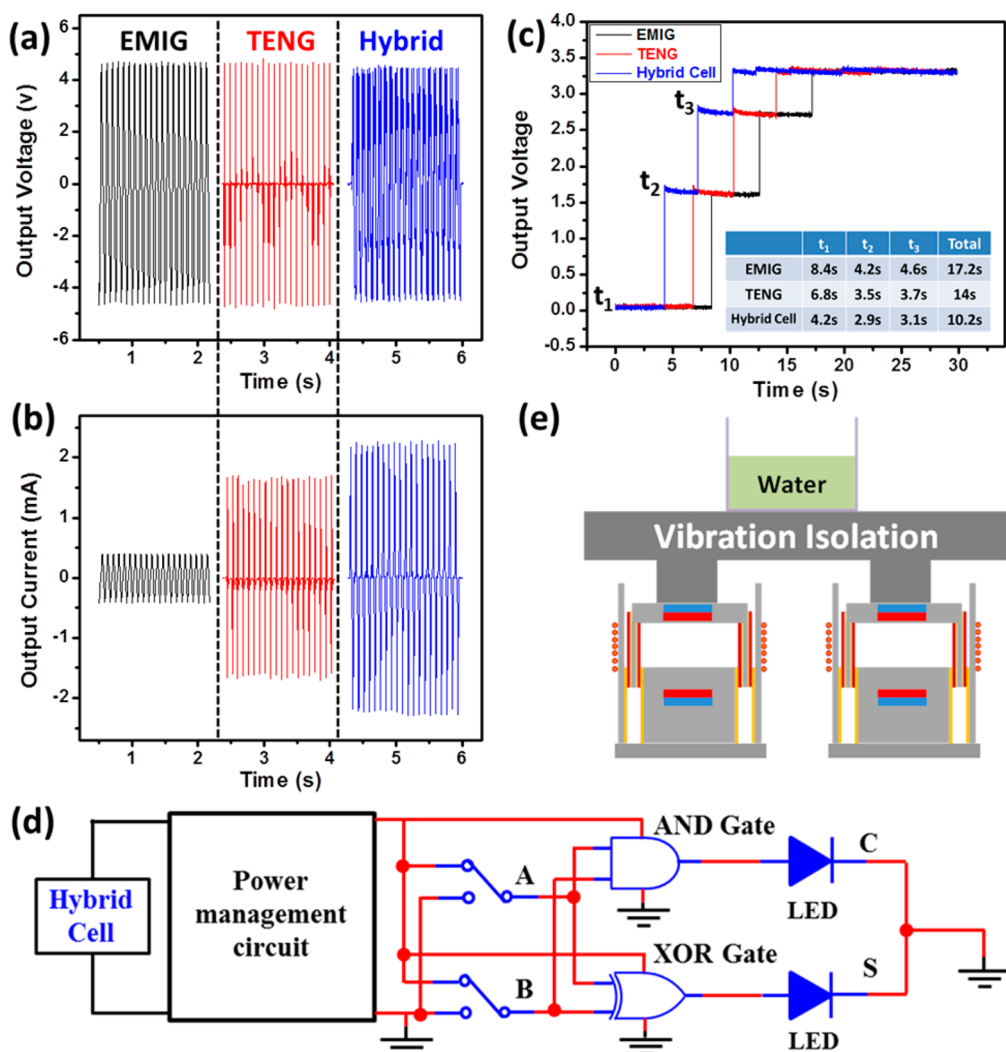
Figure 6. After impedance match, the (a) output voltage and (b) output current of the EMIG, TENG, and hybrid cell (parallel connected EMIG and TENG) on a load of 5 kΩ. (c) Voltage curves showing the charging process of a commercial buck convertor board by the EMIG, TENG, and hybrid cell to convert the ac signal into a regulated dc voltage. There are three steps. The inset table lists the times used for each step in three cases. (d) Circuit diagram for using the hybrid cell to drive a half-adder circuit and also provide the input digit signals. (e) Schematic diagram showing the construction of the hybrid cell to work as a vibration isolator.

load of 5 kΩ, as shown in Figure 6a and b. The output current in the EMIG and TENG in this case is about 0.4 and 1.6 mA, respectively. When these two parts were connected in parallel, the output voltage was maintained, and the output current increased to 2.2 mA, which is a little larger than the sum of the output currents from the EMIG and TENG. This is because the output current peaks from the EMIG are broader than the peaks from the TENG due to the different energy conversion processes for the EMIG and TENG. In this situation, when these two signals are added, the integrated area under the current peak from the hybrid cell should be the sum of those from the EMIG and TENG, which represent the total charges transferred in each cycle. This is the case in our devices. Therefore, we got a signal peak with a moderate width, and the current level is a bit higher than the sum of currents from the EMIG and TENG.

In many applications, the ac signal generated from the hybrid cell is not suitable for direct use, such as some electronic devices driven by a dc power source. To convert the hybrid cell's ac signal into a regulated voltage with a constant current supply, a commercial power management circuit board (LTC3588-1, Linear Technology) was used to regulate the power output. A schematic circuit diagram of the power management circuit is available in the Supporting Information. On this board, there is a low-loss full-wave bridge rectifier, several capacitors for energy storage, and a high-efficiency buck converter. The ac signals are first rectified by the full-wave bridge, and the charges are stored in the capacitors. A regulated output voltage of 3.3 V was achieved. Figure 6c shows the charging curves of the board. To get the 3.3 V regulated output voltage, it takes three steps. In the first step, the output voltage increased to 1.6 V, then it increased to 2.7 V,

and finally the output voltage reached 3.3 V. When we used the EMIG to drive the board individually, these three steps took 8.4, 4.2, and 4.6 s, respectively, and a total time of 17.2 s was used to get the 3.3 V output voltages, as shown in the inset table in Figure 6c. When we used the TENG individually, the time taken for each step and the whole process was decreased, as the TENG has a higher output power than the EMIG. When the EMIG and TENG work simultaneously, the time for the whole charging process was reduced to 10.2 s. After regulating the power output, the hybrid cell can be used to drive a half-adder circuit, which is an important combinational circuit in computers and other kinds of processors used for arithmetic logic units, address calculations, table indices, and similar operations. A half-adder adds two inputs, A and B, and has two outputs, sum (S) and carry (C). The carry signal represents an overflow into the next digit of a multi-digit addition. As shown in Figure 6d, a half-adder incorporated with an AND gate for C and a XOR gate for S is powered by the hybrid cell after regulation. At the same time, the 3.3 V regulated output signal from the buck converter board also serves as the input digit signal "1", and the ground of the board serves as the input digit signal "0". When the two inputs make a switch between "1" and "0", respectively, we can realize the additive operations of "0 + 0", "1 + 0", "0 + 1", and "1 + 1". The LED at the output S or C will light up when bit "1" is received at that terminal. Video 1 in the Supporting Information shows that when input A was fixed at "1", as we switched input B from "0" to "1", the LEDs at output S and C were lit up successively. It shows that we realized the logic operation successfully by using our hybrid cell as a dc power source and input digit signals.

Vibrations are common mechanical phenomena that can be found in the ambient environment. In many cases, vibration is undesirable and harmful in mechanical structures. One application of the hybrid cell working as vibration isolator or damper was demonstrated. The vibration isolation construction is shown in Figure 6e. A small table with two supports was built up with an acrylic sheet. These two supports were mounted on two hybrid cells' floating part. The test was carried out by using an electrodynamic shaker (Labworks ET-139) (see Video 2 in Supporting Information). First a beaker containing water was put on the shaker to check the vibration intensity. The water spilled out from the beaker due to the vibration transferred from the shaker. Then the beaker was put on the vibration isolation structure and then mounted on the shaker. In this condition, two hybrid cells adsorbed a large amount of vibration energy, and the water in the beaker stayed very calm. It shows a very good vibration isolation/damping effect. Furthermore, the absorbed vibration energy can be converted to electric energy by the hybrid cell to drive 16 LEDs simultaneously.

CONCLUSIONS

In conclusion, a newly designed hybrid cell is first developed by integrating a TENG and EMIG for high-efficient harvesting of mechanical energy from mechanical friction and electromagnetic induction. Both a sliding-mode and contact-mode TENG can be realized in the integrated structure. It extends the previous definition of a hybrid cell to using one device for harvesting the same type of energy through multiple approaches. The suspended structure in the hybrid cell oscillates in respond to an external disturbance. On the basis of the design, the output signals from the TENG and EMIG are in phase so that they can be added directly and constructively. The impedance match between different parts in a hybrid cell was realized for the first time by using transformers. This can reduce the power consumption in the power source itself and enhance the power transfer capability. A maximum instantaneous output power of 7.7 and 1.9 mW on a matched load of 5 kΩ was obtained for the TENG and EMIG, respectively. By using a power management circuit, the original ac signal was converted into a dc output with a regulated voltage of 3.3 V. Using the hybrid cell as both the power source and the input digit signals for logic operation was demonstrated for the first time on a half-adder circuit, which is an important combinational circuit in computers and other kinds of processors. A vibration isolation structure was constructed by using the hybrid cell, which demonstrates its great application potentials in vibration detectors, vibration dampers, vibration triggers, *etc*.

METHODS

Fabrication of a Hybrid Cell with a Sliding-Mode TENG. The hybrid cell was constructed with an acrylic sheet. First, a larger hollow cube with an opening at the top was assembled. Copper foils were used to cover the lower part of the inner surfaces. Then, a solid cube embedded with a magnet was fixed on the bottom. Its side wall surfaces are all covered with copper foils. After that, a smaller hollow cube with an opening in the bottom was constructed, and another magnet was embedded in the top board. Both the inner and outer surfaces of the cube were covered with Kapton films. The exposed surface of the Kapton film was dry-etched by using inductively coupled plasma to create aligned nanowire structures. The unexposed surface is sputtered with a thin copper film. Then, the smaller hollow cube was inserted into the larger hollow cube. The structure design ensures that the space between the solid cube and the large hollow cube is just the small hollow cube's side wall thickness, which guarantees good friction contact between the attached copper foils' and Kapton films' surfaces. The two magnets were assembled to produce a repulsive force to float the smaller hollow cube. Then the outer surface of the larger hollow cube was wrapped with a varnished wire with 300 turns to serve as the coils in the EMIG.

Supporting Information Available: A schematic circuit diagram of the power management circuit is included. Also two videos recorded for using a hybrid cell to drive a half-adder circuit for logic operation and construct vibration isolator are included. This material is available free of charge *via* the Internet at http://pubs.acs.org.

REFERENCES AND NOTES

1. Amirtharajah, R.; Chandrakasan, A. P. Self-Powered Signal Processing Using Vibration-Based Power Generation. *IEEE J. Solid-State Circ.* **1998**, *33*, 687–695.
2. Williams, C. B.; Yates, R. B. Analysis of Micro-electric Generator for Microsystems. *Sens. Actuators, A: Phys.* **1996**, *52*, 8–11.
3. Meninger, S.; Mur-Miranda, J. O.; Amirtharajah, R.; Chandrakasan, A. P.; Lang, J. H. Vibration-to-Electric Energy Conversion. *IEEE Trans. VLSI. Syst.* **2001**, *9*, 64–76.
4. Roundy, S.; Wright, P. K.; Rabaey, J. A Study of Low Level Vibrations as a Power Source for Wireless Sensor Nodes. *Comput. Commun.* **2003**, *26*, 1131–1144.
5. Glynne-Jones, P.; Beeby, S. P.; White, N. M. Towards a Piezoelectric Vibration-Powered Microgenerator. *IEE Proc.-Sci. Meas. Technol.* **2001**, *148*, 68–72.
6. Roundy, S.; Leland, E. S.; Baker, J.; Carleton, E.; Reilly, E.; Otis, B.; Rabaey, J. M.; Wright, P. K.; Sundararajan, V. Improving Power Output for Vibration-Based Energy Scavengers. *IEEE Pervas. Comput.* **2005**, *4*, 28–36.
7. Wang, Z. L.; Song, J. H. Piezoelectric Nanogenerators Based on Zinc Oxide Nanowire Arrays. *Science* **2006**, *312*, 242–246.
8. Hu, Y. F.; Zhang, Y.; Xu, C.; Lin, L.; Snyder, R. L.; Wang, Z. L. Self-Powered System with Wireless Data Transmission. *Nano Lett.* **2011**, *11*, 2572–2577.
9. Zhu, G.; Wang, A. C.; Liu, Y.; Zhou, Y. S.; Wang, Z. L. Functional Electrical Stimulation by Nanogenerator with 58 V Output Voltage. *Nano Lett.* **2012**, *12*, 3086–3090.
10. Fan, F. R.; Tian, Z. Q.; Wang, Z. L. Flexible Triboelectric Generator!. *Nano Energy* **2012**, *1*, 328–334.
11. Wang, S. H.; Lin, L.; Wang, Z. L. Nanoscale Triboelectric-Effect-Enabled Energy Conversion for Sustainably Powering Portable Electronics. *Nano Lett.* **2012**, *12*, 6339–6346.
12. Zhu, G.; Chen, J.; Liu, Y.; Bai, P.; Zhou, Y. S.; Jing, Q. S.; Pan, C. F.; Wang, Z. L. Linear-Grating Triboelectric Generator Based on Sliding Electrification. *Nano Lett.* **2013**, *13*, 2282–2289.
13. Hu, Y. F.; Yang, J.; Jing, Q. S.; Niu, S. M.; Wu, W. Z.; Wang, Z. L. Triboelectric Nanogenerator Built on Suspended 3D Spiral Structure as Vibration and Positioning Sensor and Wave Energy Harvester. *ACS Nano* **2013**, *7*, 10424–10432.
14. Lin, L.; Wang, S. H.; Xie, Y. N.; Jing, Q. S.; Niu, S. M.; Hu, Y. F.; Wang, Z. L. Segmentally Structured Disk Triboelectric Nanogenerator for Harvesting Rotational Mechanical Energy. *Nano Lett.* **2013**, *13*, 2916–2923.
15. Xu, C.; Wang, X. D.; Wang, Z. L. Nanowire Structured Hybrid Cell for Concurrently Scavenging Solar and Mechanical Energies. *J. Am. Chem. Soc.* **2009**, *131*, 5866–5872.
16. Xu, C.; Wang, Z. L. Compact Hybrid Cell Based on a Convoluted Nanowire Structure for Harvesting Solar and Mechanical Energy. *Adv. Mater.* **2011**, *23*, 873–877.
17. Pan, C. F.; Guo, W. X.; Dong, L.; Zhu, G.; Wang, Z. L. Optical Fiber-Based Core-Shell Coaxially Structured Hybrid Cells for Self-Powered Nanosystems. *Adv. Mater.* **2012**, *24*, 3356–3361.
18. Xu, C.; Pan, C. F.; Liu, Y.; Wang, Z. L. Hybrid Cells for Simultaneously Harvesting Multi-type Energies for Self-Powered Micro/Nanosystems. *Nano Energy* **2012**, *1*, 259–272.
19. Yang, Y.; Zhang, H. L.; Zhu, G.; Lee, S.; Lin, Z. H.; Wang, Z. L. Flexible Hybrid Energy Cell for Simultaneously Harvesting Thermal, Mechanical, and Solar Energies. *ACS Nano* **2013**, *7*, 785–790.
20. Zhang, C.; Tang, W.; Han, C. B.; Fan, F. R.; Wang, Z. L. Theoretical Comparison, Equivalent Transformation, and Conjunction Operations of Electromagnetic Induction Generator and Triboelectric Nanogenerator for Harvesting Mechanical Energy. *Adv. Mater.* **2014**, *26*, 3580–3591.
21. Fan, F. R.; Tang, W.; Yao, Y.; Luo, J. J.; Zhang, C.; Wang, Z. L. Complementary Power Output Characteristics of Electromagnetic Generators and Triboelectric Generators. *Nanotechnology* **2014**, *25*, 135402.
22. Niu, S. M.; Liu, Y.; Wang, S. H.; Lin, L.; Zhou, Y. S.; Hu, Y. F.; Wang, Z. L. Theory of Sliding-Mode Triboelectric Nanogenerators. *Adv. Mater.* **2013**, *25*, 6184–6193.
23. Niu, S. M.; Wang, S. H.; Lin, L.; Liu, Y.; Zhou, Y. S.; Hu, Y. F.; Wang, Z. L. Theoretical Study of Contact-Mode Triboelectric Nanogenerators as an Effective Power Source. *Energy Environ. Sci.* **2013**, *6*, 3576–3583.